CHEMISTRY
A EUROPEAN JOURNAL

DABCO-Directed Self-Assembly of Bisporphyrins (DABCO = 1,4-Diazabicyclo[2.2.2]octane)

Pablo Ballester,*[a, b] Antoni Costa,[b] Ana M. Castilla,[b] Pere M. Deyà,[b] Antonio Frontera,[b] Rosa M. Gomila,[b] and Christopher A. Hunter*[c]

Dedicated to Professor Julius Rebek, Jr., on the occasion of his 60th birthday

Abstract: Three isomeric zinc bisporphyrins have been prepared by covalently linking together two aminoporphyrins with an isophthalic acid derivative. The porphyrins differ in the substitution pattern on the *meso* phenyl groups, that is, *ortho*, *meta*, or *para*. Titrations carried out by UV-visible and ^{1}H NMR spectroscopy have been used to map out the stabilities and the stoichiometries of the complexes formed with 1,4-diazabicyclo[2.2.2]octane (DABCO) in chloroform. The *ortho*- and *meta*-substituted bisporphyrins form 1:1 intramolecular sandwich complexes. The *para*-substituted bisporphyrin cannot adopt the cofacial conformation required for this type of complex and forms a higher order 2:2 intermolecular assembly, which is stable over a wide range of DABCO concentrations.

Keywords: coordination modes · porphyrinoids · receptors · self-assembly · zinc

Introduction

Self-assembly can be considered as an algorithm that translates covalent connectivity into tertiary structure.[1] This enables the shape and size of the resulting assembly to be specified by the covalent connectivity between the interacting centers and by the geometric features of the interactions used for its construction. While nature uses a plethora of relatively weak noncovalent interactions within each assembly, our mastery of these interactions is in an early stage of development. The covalent coordination bonds formed by transition-metal centers are an attractive and simpler alternative for directing the formation of complex structures. This strategy has evolved into one of the most widely used for organizing building blocks into supramolecular arrays. Several strategies have been explored in the use of metal–ligand interactions as the driving force for the assembly of supramolecular structures.[2] In particular, the directional bonding approach, or the "Molecular Library Model" as coined by Stang,[3] has recently allowed the design and preparation of increasingly sophisticated supramolecular assemblies of porphyrins.[4] Hence, porphyrins and metalloporphyrins can be exploited in two ways as modules for the construction of the assembly. Porphyrins can act as donor building blocks provided that the periphery has ligands that can suitably coordinate to metal centers. Metalloporphyrins can act as acceptor building blocks provided that the metal atom inside the porphyrin core has at least one axial site available for coordination. Both features can be incorporated in a metalloporphyrin structure yielding a module capable of acting simultaneously as a donor and acceptor.[5] If the donor ligand complements the acceptor metal center and the covalent connectivity between the two sites is appropriate, a particular case of self-assembly can arise, that is, self-coordination (Figure 1). By using self-coordination

[a] Prof. P. Ballester
Institució Catalana de Recerca i Estudis Avançats (ICREA) and
Institut Català d'Investigació Química (ICIQ)
Avgda. Països Catalans, s/n, 43007-Tarragona (Spain)
Fax (+34) 977-920-221
E-mail: pballester@iciq.es

[b] Prof. P. Ballester, Prof. A. Costa, A. M. Castilla, Prof. P. M. Deyà, Dr. A. Frontera, R. M. Gomila
Departament de Química
Universitat de les Illes Balears
07122 Palma de Mallorca, Illes Balears (Spain)

[c] Prof. C. A. Hunter
Centre for Chemical Biology
Krebs Institute for Biomolecular Science
Department of Chemistry, University of Sheffield
Sheffield S3 7HF (UK)
Fax: (+44) 114-222-9346
E-mail: c.hunter@sheffield.ac.uk

Supporting information for this article is available on the WWW under http://www.chemeurj.org/ or from the author and contains the ^{1}H NMR spectra of **5a–c**.

DOI: 10.1002/chem.200400772

methodology, it has been possible to construct homo-oligomeric complexes of discrete macrocyclic structures[6] as well as linear architectures.[7] The covalent connectivity between the interacting centers and the number of vacant binding sites on the metal dictate the shape and number of units involved in the resulting assembly. It is known that in these cases concentration plays a pivotal role in the speciation of self-assembled structures.[8]

Heteromeric complexes are formed when bidentate ligands are used to direct the self-assembly of metalloporphyrins. The bidentate ligand 1,4-diazabicyclo[2.2.2]octane (DABCO) has been used in combination with zinc–porphyrin oligomers to form a large number of supramolecular complexes through axial coordination.[9] During our research aimed at the modular assembly of porphyrin sandwiches as potential hosts featuring an internal cavity,[10] we became interested in studying how subtle changes in the covalent connectivity of flexible zinc–bisporphyrins would translate into differences in the tertiary structures (shape and number of components) of the complexes assembled with DABCO. Such structures are the starting point for understanding the behavior of more elaborate assemblies with potential applications as molecular hosts.

Here, we describe the binding properties of a series of flexible isomeric zinc bisporphyrins (**5a–c**) in the presence of DABCO. The zinc–porphyrin/DABCO system has been widely studied by Sanders, Anderson and co-workers.[11] A simple zinc–porphyrin at micromolar concentrations forms a 1:1 complex exclusively with an association constant of about $10^5\,\text{M}^{-1}$ in organic solvents. At millimolar concentrations and when 0.5 equivalents of DABCO are present, a 1:2 DABCO–porphyrin sandwich complex is formed that opens up to give the 1:1 complex in the presence of excess DABCO (Figure 2).

The 1:2 DABCO–porphyrin sandwich motif has been used to assemble zinc–porphyrin dimers into intermolecular "ladders"[1a–c] or cofacial intramolecular complexes[9a,b] at micromolar concentrations. The intermolecular complexes are stable in the presence of a moderate excess of DABCO, and the intramolecular ones can resist higher DABCO concentrations. Increasing the DABCO concentration finally breaks down the sandwich complexes yielding open 2:1 complexes (Figure 3).

The series of zinc–bisporphyrins share the same spacer, but the conformational possibilities differ due to different substitution patterns in the aminophenyl group of the por-

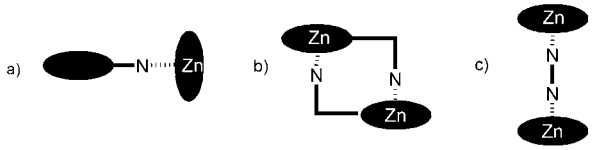

Figure 1. Schematic representation of porphyrins used for the construction of simple supramolecular complexes. a) Porphyrin with a ligand covalently incorporated into its structure acting as donor unit and a zinc–porphyrin as the acceptor unit. b) Zinc–porphyrin with covalently attached ligand that binds the zinc. c) Complex assembled using a zinc–porphyrin as acceptor and a bidentate non-porphyrin ligand.

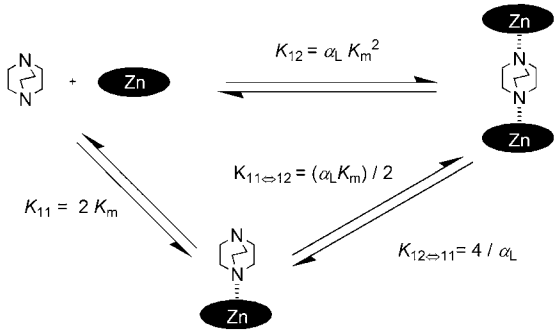

Figure 2. Schematic representation of the species involved in the equilibria of binding DABCO to a simple zinc–porphyrin. The overall binding constant K_{12} and the stepwise constants, K_{11}, $K_{11\Rightarrow12}$, and $K_{12\Rightarrow11}$, are shown as well as their relationship with K_m (the microscopic binding constant), α_L (the ligand cooperativity factor), and statistical correction factors.

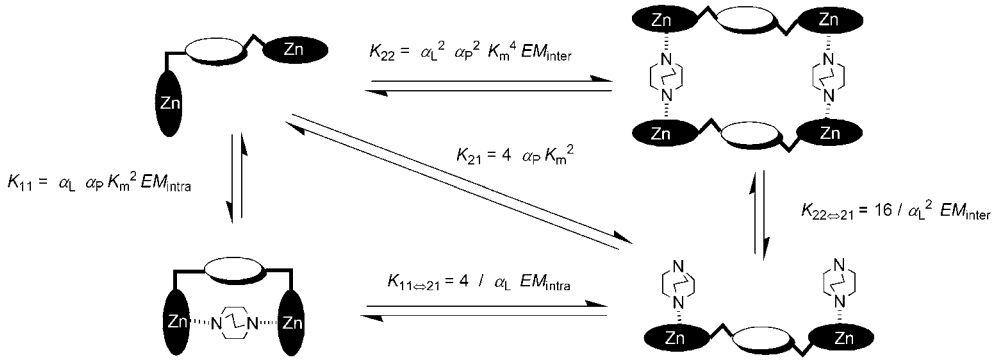

Figure 3. Schematic representation of the possible equilibria involved in the binding of DABCO to a zinc–bisporphyrin. *EM*s are the effective molarities for the intramolecular or intermolecular interaction required for cyclization. Overall stability constants (K_{21} and K_{22}) and stepwise equilibrium constant (K_{11}, $K_{11\Rightarrow21}$, and $K_{22\Rightarrow21}$) are shown and related to K_m (microscopic binding constant), *EM*, α_L (cooperativity factor of the ligand), α_P (cooperativity factor of the porphyrin), and statistical correction factors. The statistical correction factor for $K_{22\Rightarrow21}$ is larger, because two 2:1 complexes are generated for every assembly that opens up.

phyrin unit. We have studied the DABCO-induced self- and disassembly processes by means of UV-visible and ^{1}H NMR spectroscopy. The covalent connectivity in one of the bisporphyrins is suitable for building a 2:2 multicomponent assembly with DABCO. The other two bisporphyrins tend to form intramolecular cofacial sandwich complexes with DABCO. The formation of intramolecular complexes clearly limits the utility of the last two bisporphyrins in multicomponent assemblies.

Results and Discussion

Synthesis: The three isomeric aminoporphyrins **1a–c** were prepared according to the literature.[12] We note that the major product in the three condensation reactions used to prepare the porphyrin skeleton is the tetraalkylporphyrin **$H_2$2**. 5-Methoxy-1,3-benzenedicarbonyl dichloride[13] (**3**) was prepared in three steps from commercially available dimethyl 5-hydroxyisophthalate. First, the phenol was methylated by heating to reflux in dimethyl formamide and treating it with methyl iodide and cesium carbonate. Next, the methyl esters were hydrolyzed with sodium hydroxide solution followed by acidification with hydrochloric acid to furnish the corresponding diacid. Finally, reaction of the diacid in refluxing thionyl chloride afforded the dichloride **3**, which was recrystallized from hexane. Coupling with aminoporphyrins **1a–c** was accomplished by dropwise addition of a solution of **3** in methylene chloride into a solution containing one equivalent of the porphyrin and excess of triethylamine (Scheme 1). Column chromatography of the crude products allowed the recovery of unreacted porphyrin and isolation of the bisporphyrins **4a–c** as purple solids in approximately 40% yield. Metallation was accomplished in almost quantitative yield by using a solution of zinc acetate in CH_2Cl_2/MeOH (3:1) giving the zinc bisporphyrins **5a–c** and the zinc tetraalkylporphyrin **2**.

Model complexes: Before examining the DABCO complexes of the bisporphyrins, we investigated the properties of simple systems which cannot assemble into higher order structures. This was done in order to fully characterize all of the relevant binding interactions: complexation of monomeric porphyrin **2** with DABCO and the monodentate analogue quinuclidine, and complexation of bisporphyrins **5a–c** with quinuclidine.[1a,11] The coordination of DABCO to **2** was first probed by UV-visible titration in chloroform (Figure 4). Under these dilute conditions (porphyrin concentration $\approx 10^{-6}$ M), binding of DABCO results in a shift in the Soret band from 420 to 430 nm, typical of formation of a 1:1 DABCO·**2** complex. Analysis of the binding isotherm with a 1:1 binding model gave a stoichiometric[14] binding constant of $K_{11} = 1.8 \times 10^5\,\mathrm{M}^{-1}$. DABCO has two identical binding sites, so for comparison purposes with, for example, quinuclidine, the statistically corrected (microscopic) association constant should be used. Thus the microscopic association constant for the reference interaction in chloroform is $K_m = K_{11}/2 = 8.9 \times 10^4\,\mathrm{M}^{-1}$.

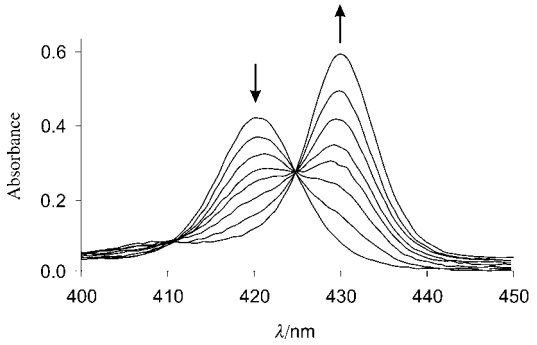

Figure 4. UV-visible titration data for **2** with DABCO showing the Soret band shift from 420 to 430 nm. Number of equivalents added: 0, 0.5, 1, 1.5, 2, 2.9, 4.8, 9.

When this system was probed by ^{1}H NMR spectroscopy (porphyrin concentration $\approx 10^{-3}$ M), free **2**, the 1:2 complex, and the 1:1 complex were observed in slow exchange at low temperatures (Figure 5). At 240 K in $CDCl_3$, in the presence of less than 0.5 equivalents of DABCO, unbound **2** and DABCO·$\mathbf{2}_2$ were observed in slow exchange. At 0.5 equivalents of DABCO, DABCO·$\mathbf{2}_2$ was the major species detected in the ^{1}H NMR spectrum. When more than 0.5 equivalents of DABCO were added, the system moved into fast exchange at 240 K. However on cooling to 220 K, the slow-exchange spectrum was obtained, and it was possible to directly observe the DABCO·$\mathbf{2}_2$ and DABCO·**2** complexes. As the DABCO concentration increased, the equilibrium gradually shifted to favor the

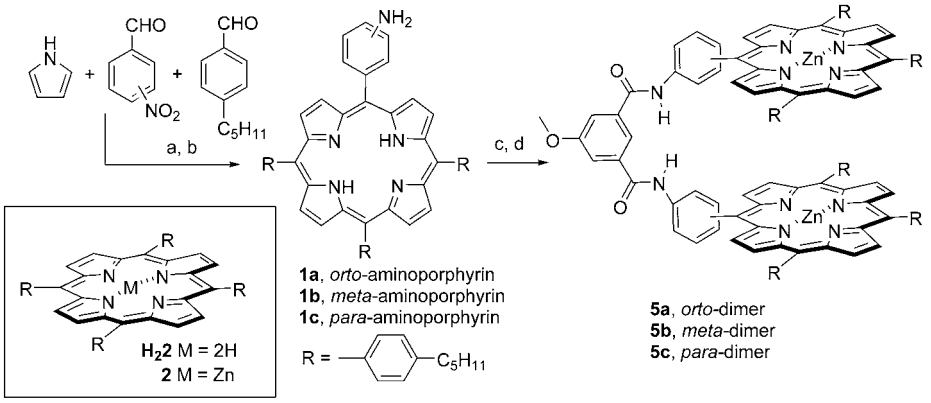

Scheme 1. a) EtOH, $BF_3{\cdot}OEt_2/CH_2Cl_2$, RT, 1 h, then dichlorodicyanobenzoquinone (DDQ) 90 min followed by Et_3N and column chromatography; b) $SnCl_2$/dioxane, 70 °C; c) 5-methoxy-1,3-benzenedicarbonyl chloride (**3**)/CH_2Cl_2, 0 °C to RT; d) $Zn(OAc)_2$ in CH_2Cl_2/MeOH (3:1).

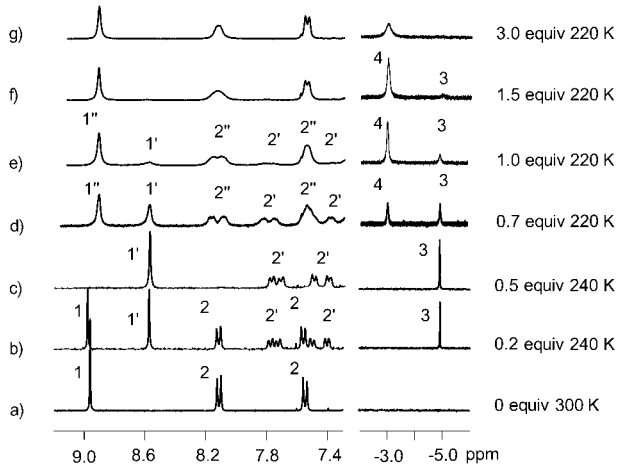

Figure 5. Selected regions of the ^{1}H NMR spectra recorded during a titration of **2** with DABCO at different temperatures. ([**2**] $=1\times10^{-3}$ M, $CDCl_3$, 300 MHz). Signals labeled 1 and 2 represent the β-pyrrole and the aromatic protons, respectively, of free **2**; primed numbers indicate the same signals in the DABCO·$\mathbf{2}_2$ complex and double primed numbers are used for those signals in the DABCO·**2** complex; signals labeled 3 represent the methylene protons of DABCO in the DABCO·$\mathbf{2}_2$ complex; those labeled 4 represent the DABCO methylene protons in the α-position with respect to the nitrogen atom that is bound to the zinc–porphyrin in the DABCO·**2** complex. The small differences in chemical shift observed for the same proton types in two different spectra are due to the changes in temperature.

DABCO·**2** complex. The signal of the β-pyrrole protons in the 1:2 sandwich complex was shifted upfield relative to the corresponding signal in free **2** or in the 1:1 complex. This was due to the proximity of the two porphyrin π-systems in the sandwich complex, causing the signal to experience a large ring-current-induced shift. At low temperatures, the two *ortho* and the two *meta* aromatic protons of the *meso* phenyl groups of the DABCO·$\mathbf{2}_2$ and DABCO·**2** complexes became nonequivalent, and the signals split into two doublets. Similar splitting has often been observed in porphyrin systems with nonequivalent faces. When ligand exchange becomes fast on the NMR timescale, the faces of the porphyrin are no longer differentiated, and averaged signals are observed for these protons. The DABCO·$\mathbf{2}_2$ ternary complex was characterized by a signal at −5 ppm, corresponding to the methylene protons of a DABCO molecule bound between two zinc–porphyrin units.[9a] When more than 0.5 equivalents of DABCO were added, a new signal appeared at −3 ppm, which is indicative of the formation of the binary complex DABCO·**2** and can be assigned to the methylene protons in the α-position with respect to the nitrogen bound to the zinc–porphyrin complex.[11a,b] The signal at −3 ppm increased at the expense of that at −5 ppm. Finally, the signal at −3 ppm broadened as the exchange became faster. The exchange rates are proportional to the concentrations of free ligand and DABCO·**2** complex, suggesting a bimolecular process in which one molecule of DABCO displaces another from the zinc atom in a concerted manner.

The association constant for formation of the DABCO·$\mathbf{2}_2$ complex K_{12} was too high to be measured accurately at NMR concentrations. However, these titrations can be used to quantify the cooperativity between the two sites of the divalent ligand DABCO, $\alpha_L=4\,K_{11=12}/K_{11}$, that is the ratio of the statistically corrected association constants for the stepwise formation of the DABCO·$\mathbf{2}_2$ complex (Figure 2).[15] At 303 K, the system was in fast exchange on the NMR timescale at all ligand-to-porphyrin ratios. The low-temperature NMR experiments showed that up to 0.5 equivalents of DABCO, the DABCO·$\mathbf{2}_2$ sandwich complex was predominantly formed, and this then opened up to form the DABCO·**2** complex with excess DABCO. By monitoring the changes in chemical shift during this second phase of the titration at 303 *K*, $K_{12=11}=4/\alpha_L$ (Figure 2) could be determined by simulation analysis of the binding isotherm following a procedure described by Anderson.[11c] The value of $\alpha_L=0.8\pm0.2$ indicates that there is rather little cooperativity in the sandwich complex. The system does not show signs of steric interaction between the *meso*-aryl substituents on binding the second zinc–porphyrin unit at the second nitrogen atom of DABCO.

We also studied the binding of quinuclidine to **2** and **5a–c** in chloroform by spectrophotometric titration. All the binding constants were calculated by using a multivariate global factor analysis of the whole series of spectra, and the results are summarized in Table 1.[16] Titration with **2** showed simple isosbestic behavior, so the data were analyzed in terms of two colored species (free **2** and the 1:1 complex). As expected, the association constant for the quinuclidine·**2** complex ($8\times10^4\,M^{-1}$) is practically identical to the value of K_m measured for the DABCO·**2** complex ($8.9\times10^4\,M^{-1}$).

Table 1. Macroscopic (K) and microscopic (K^c) binding constants for quinuclidine complexes with **2** and **5a–c**.

	K_{11} [$10^5\,M^{-1}$]	$K_{11=21}$ [$10^4\,M^{-1}$]	K_{21} [$10^9\,M^{-2}$]	K_1^{c}[a] [$10^4\,M^{-1}$]	K_2^{c}[b] [$10^4\,M^{-1}$]	α_P[c]
2	0.80±0.20	–	–	–	–	–
5a	0.80±0.40	5.0±2.5	4.0±0.5	4.0±2.0	10.0±5.0	0.4±0.1
5b	1.2±0.5	3.8±1.4	4.5±0.5	6.0±2.5	7.6±2.8	0.8±0.2
5c	1.5±0.6	4.3±1.5	6.4±1.3	7.5±3.0	8.6±3.0	0.9±0.2

[a] $K_1^c=K_{11}/2$. [b] $K_2^c=2K_{11=21}$. [c] $\alpha_P=K_{11}/4K_{11=21}=K_1^c/K_2^c$.

Zinc–porphyrin dimers often aggregate even at the low concentrations used in UV spectroscopy, but dilution studies of **5a–c** in the concentration range of 10^{-5}–10^{-7} M showed no evidence of this. The titration of quinuclidine with **5c** gave clear isosbestic spectra, but the titrations with **5a** and **5b** were non-isosbestic. The non-isosbestic behavior therefore reflects differences in the properties of the 1:1 and 2:1 complexes formed with quinuclidine. The titration data were analyzed by considering three independent colored species (free, 1:1 and 2:1; see Figure 6). The microscopic value of the second binding constant (K_2^c) for all three bisporphyrins is very close to the value of K_{11} found for **2** ($8.9\times10^4\,M^{-1}$), but the microscopic value of the first binding constant (K_1^c) is slightly lower for **5a**.[17] There is no cooperativity for **5b**,**c**

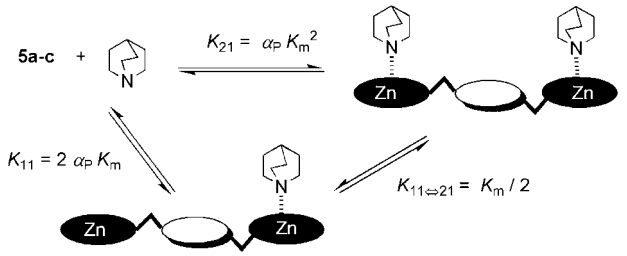

Figure 6. Schematic representation of the species involved in the equilibria of binding quinuclidine to a bisporphyrin. The overall binding constants K_{11} and K_{21}, and the stepwise constant $K_{11\rightleftharpoons 21}$ are shown and related to K_m (microscopic binding constant), α_P (cooperativity factor), and statistical correction factors.

($\alpha_P \approx 1$), but the cooperativity factor for **5a** is 0.4. Since the microscopic stability constant observed for the second binding event is similar to that observed for all of the other complexes, the cooperativity observed for **5a** is due to a destabilization of the 1:1 complex. This suggests that there is a weak intramolecular interaction between the two porphyrins in free **5a**, which is broken up by binding of the first ligand. The wavelength of the Soret band shows little indication of this interaction: $\lambda_{max} = 420.0$ nm for **5a**, 421.5 nm for **5b** and 422.0 nm for **5c** compared with 421.0 nm for the reference compound **2**. However, there are clear differences in the bandwidths: 27 nm for **5a** compared with 13 nm for **5b**, **5c**, and **2**, which provides some spectroscopic evidence for intramolecular porphyrin interactions in free **5a**.[18]

DABCO-induced self-assembly of the zinc bisporphyrins 5a–c: Addition of incremental amounts of DABCO to solutions of **5a–c** in chloroform gave a series of UV-visible spectra with more than one isosbestic phase (Figure 7).

Although the UV-visible titration spectra suggest that the three zinc bisporphyrins behave quite differently, an in depth analysis allows us to generalize. In all three cases, the initial addition of DABCO leads to a shift of the Soret absorption to approximately 426 nm (425.5, 425.0, 427.0 nm for **5a**, **5b**, and **5c**, respectively, with half bandwidths of 9, 8, and 11 nm, respectively). This 5 nm red shift of the Soret absorption is characteristic of a 1:2 DABCO–porphyrin sandwich complex.[19] On addition of more DABCO, the intensity of the absorption band at 426.0 nm decreased, and a new absorption band appeared at 431.0 nm for **5a** and **5c**. As observed for reference compound **2**, a Soret absorption at 431.0 nm is typical of a simple 1:1 DABCO–porphyrin complex. Thus, the Soret absorption at 431.0 nm for **5a** and **5b** was assigned to a 2:1 DABCO–bisporphyrin complex. In the titration of **5b**, a similar increase in the DABCO concentration caused only a slight decrease in the absorbance at 426.0 nm, and a band at 431.0 nm was not observed. Initially, all titrations gave a sharp isosbestic point as the equilibrium of the formation of the sandwich complex was the main process. However, for **5a** and **5c**, because the formation and destruction of the sandwich complex occurs in a similar ligand concentration regime (see below), the titrations indicated a non-isosbestic phase before establishing a new isosbestic point, when the equilibrium of the destruction of the sandwich complex dominated. The destruction process of the sandwich complex of **5c** occurs at a different ligand concentration and does not show a new isosbestic point.

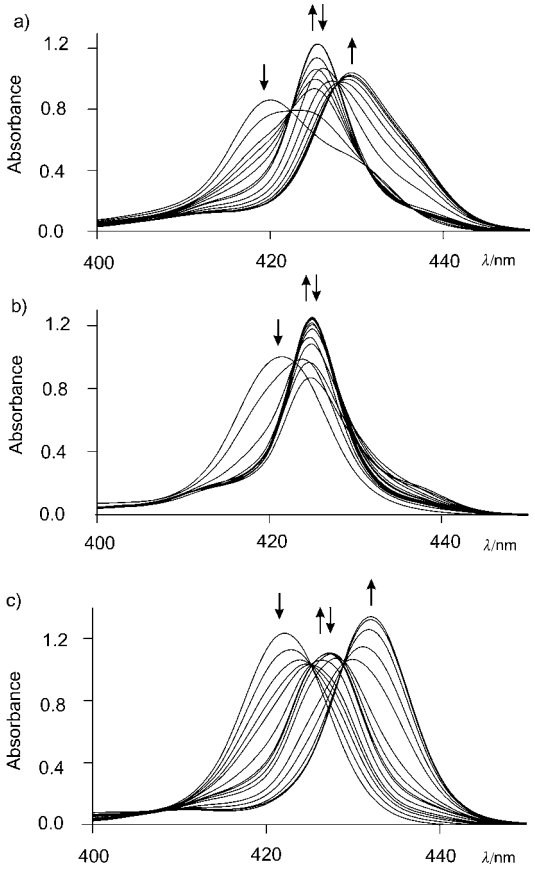

Figure 7. UV-visible titration spectra (Soret region) of **5a–c** with DABCO in chloroform at 298 K. The concentration of the bisporphyrin was maintained constant throughout the titration (1×10^{-6} M). a) **5a**. Number of equivalents of DABCO added per dimer bisporphyrin: 0, 0.12, 0.28, 0.4, 0.6, 1.1, 4, 25, 500, 1000, 2200, 4500, 7000, 12000, 120000. b) **5b**. Number of equivalents of DABCO added per bisporphyrin: 0, 0.2, 0.5, 0.7, 1, 2, 4, 100, 600, 1500, 6500, 25000, 35000, 600000, 1000000. c) **5c**. Number of equivalents of DABCO added per dimer bisporphyrin: 0, 0.15, 0.30, 0.5, 0.6, 1.2, 4, 6, 20, 60, 250, 450, 1000, 4000, 120000.

Taken together, these results suggest that there are two consecutive and different two-state equilibria and that it is valid to analyze these titrations in terms of three colored states.[1a,20] However at this stage, it is not possible to assign the stoichiometry of the sandwich complex, which could be an intramolecular 1:1 complex or an intermolecular 2:2 assembly.

Figure 8 shows the data for the titrations up to 1000 equivalents of DABCO. The binding isotherm for **5b** is a straight line with an abrupt endpoint after addition of one equivalent of DABCO, so the stability of this complex is too high to be measured at this concentration ($K > 10^7\ M^{-1}$). No further changes in the spectrum were observed until about 4000 equivalents of DABCO were added. At this point, destruction of the sandwich complex started to occur accompa-

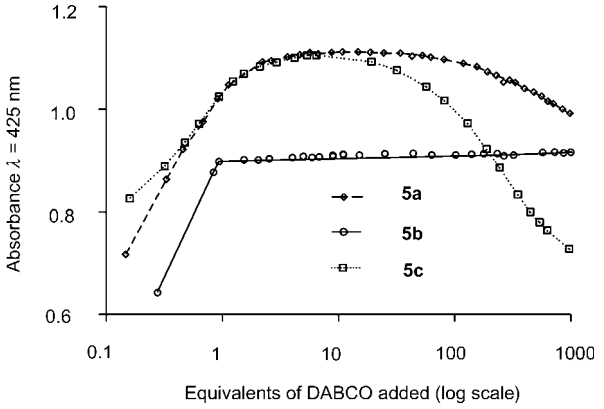

Figure 8. Spectrometric titration curves for titration of **5a** (diamonds), **5b** (circles) and **5c** (squares) with DABCO in chloroform following the change in absorbance at 425 nm.

nied by a small increase in absorption at about 431.0 nm. The titration curve for the destruction of the sandwich complex was analyzed by curve fitting as a simple two-state equilibrium, assuming that the concentration of free **5b** is negligible after one equivalent of DABCO has been added. If we assume that the sandwich complex is 1:1 DABCO·**5b**, by determining $K_{11=21}$ we can indirectly obtain an estimate for K_{11} using the thermodynamic cycle shown previously in Figure 3 ($K_{11}=K_{21}/K_{11=21}=4\,K_m^2/K_{11=21}$). The cooperativity factors for DABCO and **5b** (α_L and α_P) are unity, so the individual zinc–nitrogen interactions all have identical values to K_m (measured in control experiments as $8.9\times10^4\,M^{-1}$). If we assume that the sandwich complex is the 2:2 $(DABCO)_2$·$(\mathbf{5b})_2$ assembly, we can estimate the value of K_{22} in the same way. Due to the mathematical complexity of the model for formation of the intermolecular assembly, K_{22} was determined by using SPECFIT (see Experimental Section for details) to fit the second phase of the titration, considering all three colored species, free **5b**, the 2:2 complex, and the 2:1 complex, and fixing the value of K_{21} at $4K_m^2$.

Bisporphyrins **5a** and **5c** show rather different behavior. Figure 8 shows that the first phase of the titration process followed a shallower saturation curve that can be analyzed to provide accurate stability constants for the sandwich complexes. Here, the destruction of the sandwich complexes occurred in a similar ligand concentration regime, and the absorption at 426.0 nm started to decrease after 25 equivalents of DABCO had been added to **5a**, and after only six equivalents had been added to **5c**. We could therefore analyze the full set of titration data in terms of the three colored species: free, a 1:1 or 2:2 sandwich complex, and 2:1 open complex (Figure 3). The fitting of the whole series of spectra obtained for the titrations to two different binding models that differ in the stoichiometry of the intermediate sandwich complex, 2:2 or 1:1, revealed that the goodness of the fit cannot be used as the criterion to decide the correct binding model. Table 2 summarizes the values of the stability constants obtained using the two different models. The measured values of K_{21} give some indication of the quality and fit of the data analysis: for the titrations of **5a** and **5c**, the measured values for K_{21} are within the expected range using the relationship $K_{21}=4\alpha_P K_m^2$ ($3–7\times10^{10}\,M^{-1}$).

Table 2. Binding constants and effective molarities for complexes formed between bisporphyrins **5a–c** and DABCO for two different possible stoichiometries.

	5a	**5b**	**5c**
formation of an intramolecular 1:1 sandwich complex			
K_{21} [M^{-2}]	$(4.1\pm1)\times10^{10}$	$(3.1\pm1.2)\times10^{10}$[a]	$(4.5\pm0.5)\times10^{10}$
K_{11} [M^{-1}]	$(3.5\pm0.5)\times10^{7}$	$(2.5\pm1)\times10^{8}$[b]	$(1\pm0.1)\times10^{7}$
$K_{11=21}$ [M^{-1}]	1170 ± 330	124 ± 69[c]	4500 ± 670
EM_{intra} [M][d]	$(1.8\pm0.4)\times10^{-3}$	$(3.0\pm1.4)\times10^{-2}$	$(1.3\pm0.3)\times10^{-3}$
formation of an intermolecular 2:2 sandwich assembly			
K_{21} [M^{-2}]	$(4.5\pm1.5)\times10^{10}$	$(3.1\pm1.2)\times10^{10}$[a]	$(3.6\pm0.5)\times10^{10}$
K_{22} [M^{-3}]	$(1.5\pm1)\times10^{21}$	$(6.3\pm3)\times10^{22}$[c]	$(6.5\pm2)\times10^{19}$
$K_{22=21}$ [M^{-1}]	1.4 ± 1	$(1.5\pm1.3)\times10^{-2}$	20 ± 8
EM_{inter} [M][e]	3.6 ± 2.8	1000 ± 300	1.0 ± 0.2

[a] Calculated from $K_{21}=4\alpha_P K_m^2$. [b] Calculated from $K_{11}=4\alpha_P K_m^2/K_{11=21}$. [c] Using the data after one equivalent of DABCO had been added. [d] Calculated from $EM_{intra}=K_{11}/\alpha_L\alpha_P K_m^2$. [e] Calculated from $EM_{inter}=K_{22}/\alpha_L^2\alpha_P^2 K_m^4$.

As evidenced in Figure 3, the second interaction in the formation of the 1:1 sandwich complex and the fourth interaction in the formation of the 2:2 complex are intramolecular. Effective molarities (*EM*) or chelation factors are useful for quantifying the stabilization due to intramolecular interactions in such self-assembled structures. The values of *EM* also give an indication of the amount of binding energy that could be used for bimolecular catalysis, if it could be directed into transition state stabilization.[21] The thermodynamic effective molarity is defined as $EM_{intra}=K_{11}/\alpha_L\alpha_P K_m^2$ for the second binding interaction in the 1:1 complex, and $EM_{inter}=K_{22}/\alpha_L^2\alpha_P^2 K_m^4$ for the fourth binding interaction in the 2:2 assembly.[22] The cooperativity factor α_p is only required to account for the destabilization of the first binding event for bisporphyrin **5a**. In effect, K_1^c (Table 1) for this zinc–nitrogen interaction with quinuclidine is lower than for the others. The calculated values of *EM* shown in Table 2 fall within the previously reported range and do not help to distinguish between the two possible sandwich complexes.[23, 8b, 22] The 2:2 assembly involves two bisporphyrins and so its stability, relative to the free and 2:1 states, depends on the porphyrin concentration used to carry out the titration. In contrast, the stability of the 1:1 intramolecular complex relative to the free and the 2:1 states does not depend on porphyrin concentration. Although titration experiments at a given concentration can be fitted to either model equally well, if the 2:2 assembly is present titrations at different porphyrin concentrations should produce quite different behavior. We used the binding constants determined by fitting the UV-visible data to simulate the behavior at higher and lower porphyrin concentrations to find the concentration regime that best distinguishes the two possibilities. Figure 9 shows the simulated population profiles for **5a**. The DABCO concentration at which 50 % of **5a** is involved in a

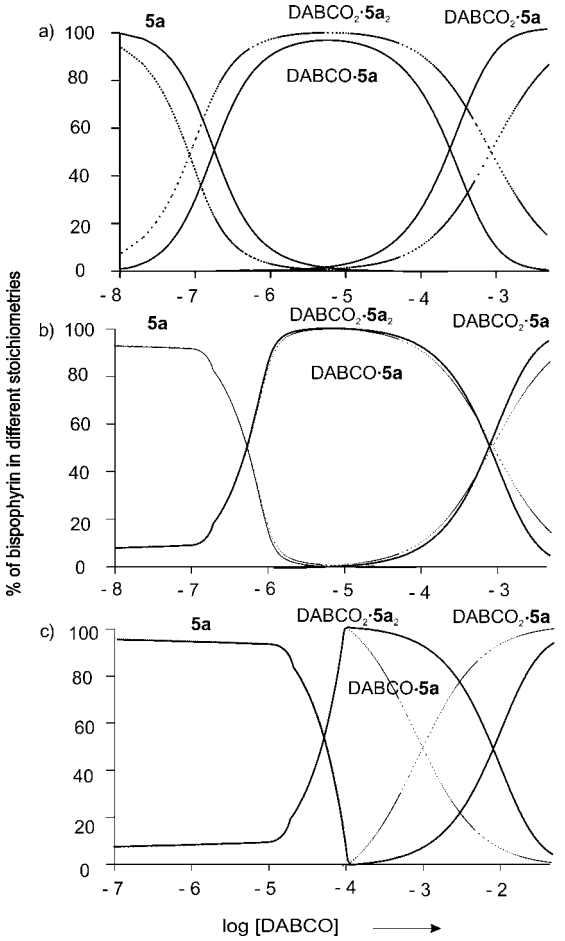

Figure 9. Simulated speciation profiles for a titration of **5a** with DABCO using the equilibrium constants in Table 2 and assuming two possible binding models (bold line formation of an intermediate intermolecular 2:2 assembly, dotted line formation of an intermediate intramolecular 1:1 complex, see Figure 3). Each profile has been plotted at a different concentration of **5a**: a) $[\mathbf{5a}]=1\times10^{-7}$ M, b) $[\mathbf{5a}]=1\times10^{-6}$ M, and c) $[\mathbf{5a}]=1\times10^{-4}$ M.

sandwich complex and the other 50% forms the open 2:1 complex is constant ($\sim10^{-3}$ M) for the intramolecular binding model, but variable in the case of the intermolecular model. In the intermolecular model, higher concentrations of **5a** require a higher concentration of DABCO to reach the halfway point. For $[\mathbf{5a}]=1\times10^{-7}$ M, $[\mathbf{5a}]=1\times10^{-6}$ M, and $[\mathbf{5a}]=1\times10^{-4}$ M, the required DABCO concentrations are approximately 5×10^{-3} M, 1×10^{-3} M, and 1×10^{-2} M, respectively.

Based on these simulations, we carried out titrations at millimolar concentrations using ^{1}H NMR spectroscopy. At room temperature and up to one equivalent of DABCO, the chemical exchange process between the free bisporphyrins and the sandwich complexes is slow on the NMR timescale. A new set of signals corresponding to the complex can be observed, and the DABCO protons at approximately $\delta=-5$ ppm are diagnostic of a sandwich complex. For porphyrins **5a** and **5c**, the free signals are broadened due to fast exchange between the free porphyrin and small amounts of a ternary sandwich complex (two bisporphyrins binding one DABCO molecule). For bisporphyrin **5b** (Figure 10), this broadening is not observed, and we conclude that in this case, the amount of ternary complex formed is negligible.[24]

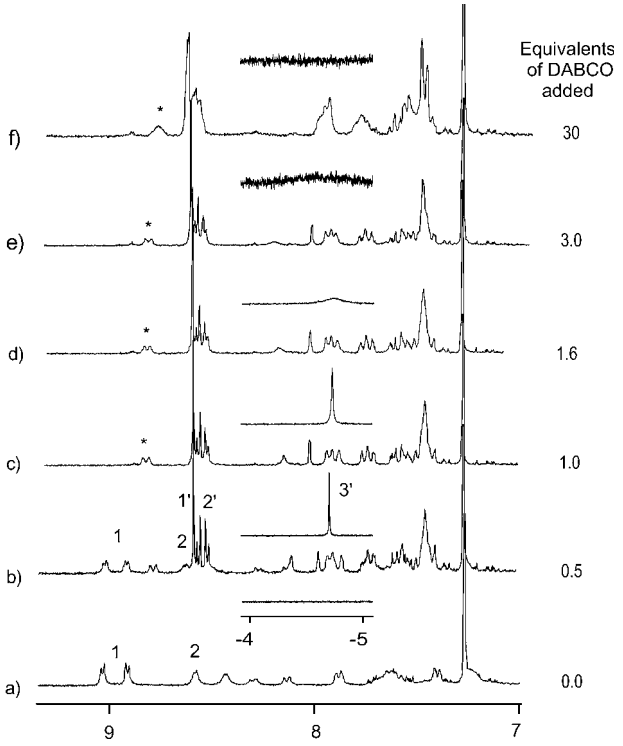

Figure 10. The aromatic region of ^{1}H NMR spectra of **5b** in the presence of increasing amounts of DABCO showing the progressive formation of the sandwich complex as a slow exchange process and its destruction as a fast exchange process. 1 and 2 are β-pyrrole protons of free **5b**; primed numbers indicate β-pyrrole protons in the respective sandwich complex. The change in chemical shift of the doublet marked with an asterisk after one equivalent of DABCO was added was used to calculate the percentage of porphyrin involved in a sandwich complex (see text). Inset: upfield region of the ^{1}H NMR spectra; 3′ indicates the methylene protons of the DABCO bound in a sandwich complex. The broadening of this signal due to chemical exchange during the titration is shown.

When one equivalent of DABCO was added, only the signals of the sandwich complex were observed. As more DABCO was added, the porphyrin protons assigned to the sandwich complex gradually shifted, indicating a fast exchange equilibrium between the sandwich complex and the 2:1 complex. For **5a** and **5b**, the signal due to bound DABCO also broadened through chemical exchange.

Similar behavior was observed for **5c**, but the onset of the second equilibrium occurred at DABCO concentrations of less than one equivalent, hinting that a different binding model was operative for this system.

The changes in chemical shift of selected porphyrin signals were analyzed in terms of a fast-exchange two-state equilibrium. We assume that after one equivalent of DABCO has been added, there is no free porphyrin in solution, and the chemical shifts at this point correspond to

the sandwich complex. The chemical shifts of the 2:1 complex can be estimated from the spectrum in the presence of large excess of DABCO or by extrapolation of the binding curve. Thus, the percentage bisporphyrin present as the sandwich complex can be calculated using the Equation (1), in which $\Delta\delta$ is the difference between the observed chemical shift and the chemical shift of the sandwich complex and $\Delta\delta_{max}$ is the difference between the chemical shifts of the sandwich and 2:1 complexes.

$$\%P_{\text{sandwich}} = \left(\frac{\Delta\delta}{\Delta\delta_{\max}}\right) \times 100 \qquad (1)$$

This equation is independent of the binding model, since the relative stoichiometry of both sandwich complexes is 1:1. At millimolar concentrations of the porphyrin, the simulated speciation profile of the sandwich complex after one equivalent of DABCO has been added is quite different depending on the stoichiometry assigned to the sandwich complex (Figure 9c and 11). Equation (1) was used to determine the amount of sandwich complex present during the NMR titrations, and this data is plotted together with simulated profiles in Figure 11.[25]

The experimental data agree very well with the simulated profile for a 1:1 complex in the cases of **5a** and **5b**. On the other hand, the experimental data for **5c** agree with the speciation profile of a 2:2 assembly. In this case, we can rule out the possibility of higher order complexes, such as the 3:3 assembly, by using the UV-visible titration data to predict the behavior at NMR concentrations (see Figure 11c). We conclude that DABCO forms simple intramolecular 1:1 complexes with **5a** and **5b** and an intermolecular 2:2 assembly with **5c**. The high effective molarities mean that these systems are stable even at millimolar concentrations in the presence of excess DABCO. Figure 12 shows the speciation diagrams for the titrations of **5c** with DABCO at micromolar and millimolar concentrations. The diagrams show the DABCO concentration range in which the 2:2 sandwich assembly exists as the major component in solution.

To gain further insight into the structures of the complexes,[26] semiempirical molecular modeling was used. No symmetry constraints were imposed and it was assumed that no side chains were attached to the bisporphyrins to keep the size of the calculation amenable. The results show that **5a** and **5b** can easily achieve conformations that place the porphyrin units in a cofacial arrangement appropriate for the formation of a 1:1 intramolecular sandwich complex with DABCO (Figure 13).

Based on AM1 calculations, the formation of DABCO·**5b** is 5 kJ mol^{-1} more favorable than the formation of DABCO·**5a**, which agrees with the difference of K_{11} values for these complexes. We have also modeled the intramolecular complex DABCO·**5c** (Figure 14). It is 54 kJ mol^{-1} less stable than DABCO·**5b**, because a cofacial arrangement of the porphyrin units can only be achieved by distorting the planarity of the amide groups. On the other hand, molecular modeling shows that **5c** can form a strain-free 2:2 assembly

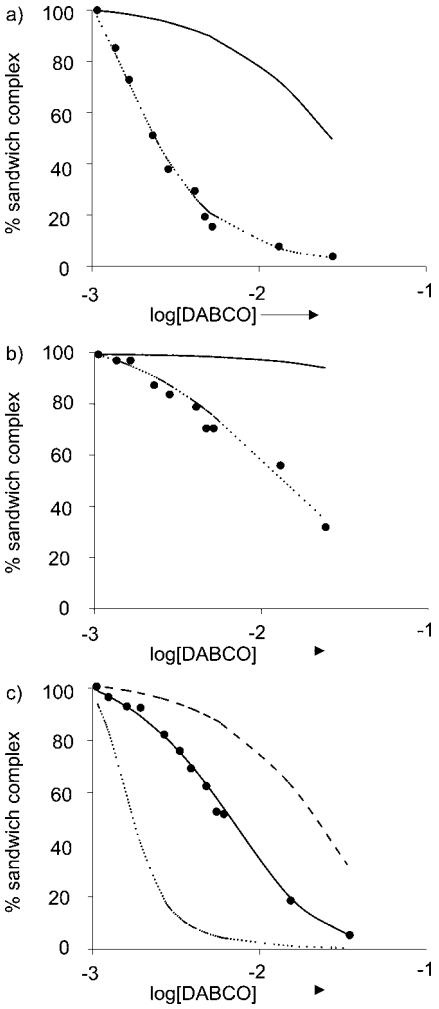

Figure 11. Simulated profiles showing the percentage bisporphyrin present as the sandwich complex, a) **5a**, b) **5b**, and c) **5c** (1×10^{-3} M). Dotted lines correspond to the destruction of a 1:1 sandwich complex, bold lines to destruction of a 2:2 complex and the dashed line in c) to destruction of a 3:3 complex. The black circles (●) were calculated from the experimental NMR data (see text).

with DABCO. This complex is 50 kJ mol^{-1} per bisporphyrin more stable than DABCO·**5c**. The 2:2 sandwich complex has a central cavity with four convergent amide N–H bonds, which augurs well for the use of this system as a molecular receptor.

The high value of the effective molarity calculated for $(DABCO)_2$·$\mathbf{5c}_2$ (1 M) is indicative of a very good complementarity in the sandwich architecture, but the key feature of this system is the very low complementarity for the intramolecular complex that dominates in the other two systems. The high value of the effective molarity also prevents competition between discrete assembly processes and oligomerization into less well-defined mixtures. These results have paved the way for the study of the DABCO-induced self-assembly of more complex systems based on trisporphyrins, as well as recognition studies on the resulting molecular assemblies. Both subjects are currently under investigations in our laboratories.

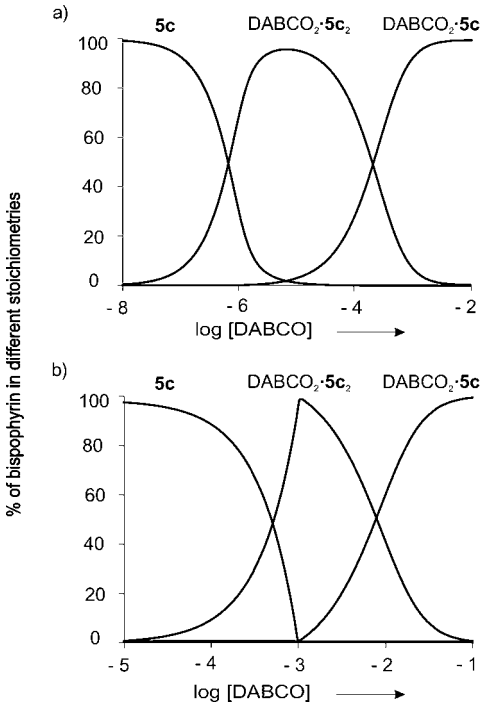

Figure 12. Simulated profiles for the titrations of **5c** with DABCO using the equilibrium constants in Table 2 for the exclusive formation of an intermolecular 2:2 sandwich assembly. Each profile has been plotted at a different concentration of **5c**: a) $[\mathbf{5c}]=1\times10^{-6}$ M and b) $[\mathbf{5c}]=1\times10^{-3}$ M.

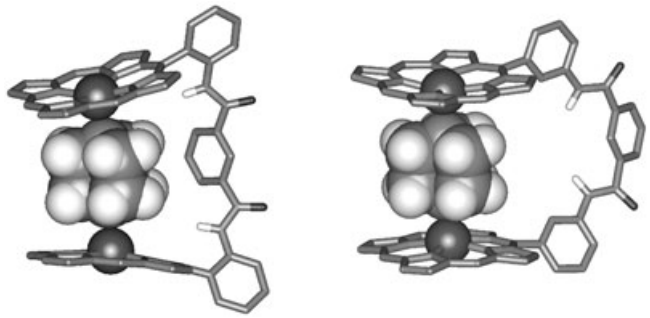

Figure 13. AM1 optimized structures of DABCO·**5a** (left) and DABCO·**5b** (right).

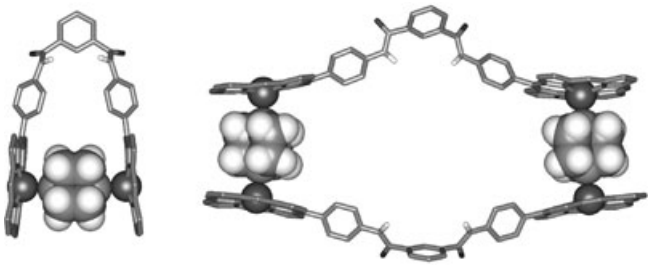

Figure 14. AM1 optimized structures of DABCO·**5c** (left) and $DABCO_2$·$\mathbf{5c}_2$ (right).

Conclusion

We have synthesized three isomeric zinc–bisporphyrins that differ in the three-dimensional arrangement of the metal binding sites and have studied the formation of molecular assemblies with the bidentate ligand DABCO. Two bisporphyrins, **5a** and **5b** form simple 1:1 intramolecular sandwich complexes with DABCO, but **5c** forms a stable 2:2 intermolecular sandwich assembly. The **5a** and **5c** sandwich complexes open up to form simple 2:1 complexes in the presence of excess DABCO, but the **5b** complex is remarkably stable and cannot be destroyed even by a large excess of DABCO. These observations were corroborated by AM1 semiempirical calculations.

The different behavior of these systems could be characterized, because we were able to study the complexation processes in detail using both UV-visible and ^{1}H NMR spectroscopy. By using a single concentration, for example, the micromolar regime used for UV-visible experiments, it is impossible to tell whether the titration data is best described by the formation of a 1:1 complex or by a higher order 2:2 assembly. The association constants determined with the UV-visible titrations can be used to simulate the binding isotherms of the two possible binding models at millimolar concentration. At this higher concentration, simple 1:1 complexation and the formation of higher order assemblies can easily be distinguished, because they lead to a quite different behavior when opening to form the 2:1 complex. The stability of the 2:2 assembly increases significantly with concentration, whereas the simple 1:1 complexes are insensitive to concentration. At millimolar concentrations, the experimental data of the destruction of the sandwich complex fits very well to the speciation profile simulated using the stability constants determined by UV-visible spectroscopy. The agreement between experimental and simulated destruction profiles at millimolar concentrations allowed us to distinguish the operative binding mode for each bisporphyrin. The stability of the assembly formed with **5c** and DABCO over a wide range of concentrations, and the fact that molecular modeling shows that the self-assembled structure has a large cavity in which four N–H bonds can converge, augurs well for potential use in host–guest chemistry.

Experimental Section

General: ^{1}H NMR spectra were recorded on a Bruker AMX-300 and Bruker AVANCE-300. Electron-spray-ionization high-resolution mass spectra (ESI MS) were obtained on a Micromass Autospec 3000. Fast-atom-bombardment mass spectra (FAB MS) were measured on a VG AutoSpec. UV-visible spectra were measured on a Varian Cary 300 Bio.

Materials: All commercial solvents and chemicals were of reagent grade quality and were used without further purification except as noted below. Deuterochloroform and chloroform were deacidified by passing through a short column of aluminium oxide 90 active, neutral (Merck). Thin-layer chromatography (TLC) and flash column chromatography were performed with DC-Alufolien Kieselgel 60 F_{254} (Merck) and Silicagel Sharlab 60, respectively. DABCO and quinuclidine were sublimed prior to use. Compounds **2** and **1a–c** were prepared as described previously.[12]

5-Methoxy-1,3-benzenedicarbonyl dichloride (3): Anhydrous cesium carbonate (1.6 g, 4.9 mmol) and iodomethane (410 μL, 6.5 mmol) were added to a solution of commercially available (Aldrich) dimethyl 5-hydroxyisophthalate (1 g, 4.75 mmol) in dry dimethyl formamide (10 mL).

The mixture was heated at 80 °C under argon atmosphere for 2 h. After cooling to room temperature, *tert*-butyl methyl ether (50 mL) was added and the solids were filtered through celite. The filtrate was washed with HCl (1 N) and brine, dried over Na_2SO_4, filtered and concentrated in vacuo, to give the crude white solid dimethyl ester of 5-methoxy-1,3-benzenedicarboxylic acid[27] (750 mg, 70 %). ^{1}H NMR (300 MHz, $CDCl_3$): δ = 8.28 (t, J = 1.2 Hz, 1 H,), 7.75 (d, J = 1.2 Hz, 2 H), 3.94 (s, 6 H), 3.89 ppm (s, 3 H).

Without any further purification, the crude product (750 mg, 3.3 mmol) was suspended in an aqueous solution of sodium hydroxide (1 N, 20 mL). The suspension was heated at 70 °C under argon atmosphere overnight, during which time the reaction mixture turned to a clear solution. The mixture was allowed to reach room temperature and was diluted with NaOH (1 N, 30 mL). The aqueous solution was extracted with *tert*-butyl methyl ether (3 × 20 mL). Concentrated HCl was added to the aqueous layer to pH ~ 3. The resulting white precipitate was collected by vacuum filtration and dried in vacuo to give 5-methoxy-1,3-benzenedicarboxylic acid as a white solid (570 mg, 88 %). M.p. 260–268 °C; ^{1}H NMR (300 MHz, $CDCl_3$/[D_6]DMSO): δ = 8.18 (t, J = 1.4 Hz, 1 H), 7.61 (d, J = 1.4 Hz, 2 H), 3.75 ppm (s, 3 H); ^{13}C NMR (75 MHz, $CDCl_3$/[D_6]DMSO): δ = 167.5, 159.4, 132.5, 123.4, 119.1, 55.6 ppm; IR (KBr): $\tilde{\nu}$ = 3415, 1704, 1464, 1421, 1384, 1279, 1057, 760, 694 cm^{-1}.

The crude diacid obtained above (570 mg, 2.9 mmol) was suspended in thionyl chloride (2 mL, 27.4 mmol), and a catalytic amount of triphenylphosphine was added. The mixture was refluxed under argon until the solid was completely dissolved (3 h) and evaporated to dryness to give a solid residue. The residue was dissolved in dry CH_2Cl_2 (5 mL) and the solvent was evaporated under reduced pressure. This process was repeated three times. The final solid residue was purified by crystallization from hexane to yield compound **3** (290 mg, 43 %) as white needles. ^{1}H NMR (300 MHz, $CDCl_3$): δ = 8.46 (t, J = 1.2 Hz 1 H), 7.89 (d, J = 1.2 Hz, 2 H), 3.95 ppm (s, 3 H); ^{13}C NMR (75 MHz, $CDCl_3$): δ = 165.5, 158.6, 133.7, 124.4, 120.6, 54.5 ppm.

General procedure for the preparation of free-base bisporphyrins 4a–c: A solution of aminoporphyrin **1** (220 mg, 0.26 mmol), freshly distilled dry triethylamine (60 μL, 0.4 mmol), and a catalytic amount of 4-(dimethylamino)pyridine (DMAP) in dry CH_2Cl_2 (30 mL) was cooled at 0 °C in an ice-water bath, and diacid **3** (31 mg, 0.13 mmol) was added in one portion. After stirring for 4 h at room temperature under argon atmosphere, the organic layer was washed with saturated $NaHCO_3$ and brine, dried over Na_2SO_4, filtered, and concentrated in vacuo to yield a solid residue. The product was separated from the unreacted porphyrin by flash chromatography of the residue on silica gel eluting with CH_2Cl_2:THF (99:1) to recover first the aminoporphyrin **1** followed by the free-base bisporhyrin **4** as a purple solid.

Free-base bis-porphyrin 4a: Yield 40 %; ^{1}H NMR (300 MHz, $CDCl_3$): δ = 8.82 (d, J = 5.7 Hz, 4 H), 8.78 (d, J = 5.7 Hz, 4 H), 8.66 (d, J = 4.7 Hz, 4 H), 8.49 (d, J = 4.7 Hz, 4 H), 8.26 (d, J = 8.2, 2 H), 8.11 (d, J = 7.2 Hz, 2 H), 7.98 (m, 8 H), 7.86 (d, J = 7.4 Hz, 4 H), 7.67 (t, J = 8.2 Hz, 2 H), 7.59 (d, J = 7.2 Hz, 4 H), 7.49 (d, J = 7.2 Hz, 4 H), 7.44 (t, J = 8.2 Hz, 2 H), 7.37(d, J = 7.2 Hz, 4 H), 6.99 (s, 2 H), 6.02 (s, 1 H), 4.66 (s, 2 H), 2.96 (t, J = 7.8 Hz, 4 H), 2.90 (t, J = 7.8 Hz, 8 H), 1.86 (m, 12 H), 1.51 (m, 24 H), 1.03 (m, 18 H), 1.0 (s, 3 H), −2.94 ppm (s, 4 H).

Free-base bis-porphyrin 4b: Yield 42 %; ^{1}H NMR (300 MHz, $CDCl_3$): δ = 8.86 (s, 8 H), 8.83 (s, 8 H), 8.32 (s, 2 H), 8.1 (m, 16 H), 7.5 (m, 19 H), 3.8 (s, 3 H), 2.95 (t, J = 7.5 Hz, 4 H), 2.88 (t, J = 7.5 Hz, 8 H), 1.85 (m, 12 H), 1.51 (m, 24 H), 1.02 (m, 18 H), −2.75 ppm (s, 4 H).

Free-base bis-porphyrin 4c: Yield 42 %; ^{1}H NMR (300 MHz, $CDCl_3$): δ = 8.89 (s, 8 H), 8.87 (s, 8 H), 8.35 (s, 2 H), 8.29 (d, J = 8.2 Hz, 4 H), 8.26 (s, 2 H), 8.12 (d, J = 8.2 Hz, 4 H), 8.11 (d, J = 7.8 Hz, 12 H), 7.84 (s, 2 H), 7.55 (d, J = 7.8 Hz, 12 H), 2.94 (t, J = 7.5 Hz, 12 H,), 1.90(m, 12 H), 1.52 (m, 24 H), 1.02 (t, J = 7 Hz, 18 H), −2.75 ppm (s, 4 H).

General procedure for the preparation of the zinc–bisporphyrins 5a–c: The free-base bisporphyrin **4** (100 mg, 0.05 mmol) was dissolved in CH_2Cl_2/CH_3OH (3:1, 30 mL) and zinc acetate (180 mg, 0.98 mmol) was added. The reaction mixture was protected from light and stirred at room temperature for 1 h. After removal of the solvents under reduced pressure, the product was purified by column chromatography on basic alumina eluting with CH_2Cl_2/CH_3OH (99:1). The product was recrystallized from CH_2Cl_2/CH_3OH yielding the zinc–bisporphyrin **5** as a purple powder.

Zn–bisporphyrin 5a: Yield 90 %; m.p. 260–268 °C; ^{1}H NMR (300 MHz,[D_5]pyridine): δ = 9.19 (d, J = 4.5 Hz, 8 H), 9.10 (s, 2 H), 9.01 (d, J = 4.9 Hz, 8 H), 8.7 (s, 2 H), 8.28 (m, 16 H), 7.79 (t, J = 7.5 Hz, 2 H), 7.61 (m, 12 H), 7.10 (s, 1 H), 5.18 (s, 2 H), 2.97 (t, J = 7.5 Hz, 4 H), 2.90 (t, J = 7.5 Hz, 8 H), 1.85 (m,12 H), 1.44 (m, 24 H), 1.00 (t, J = 7.1 Hz, 6 H), 0.95 (t, J = 7.1 Hz, 12 H), 0.94 ppm (s, 3 H); IR (KBr): $\tilde{\nu}$ = 3416, 2925, 2854, 1639, 1617, 1384, 1079, 799, 621, 476 cm^{-1}; HRMS (ESI): m/z calcd for $C_{127}H_{122}N_{10}O_3Zn_2Na$: 1989.8187; found: 1989.8251.

Zn–bisporphyrin 5b: Yield 93 %; m.p. 245–250 °C; ^{1}H NMR (300 MHz, [D_5]pyridine): δ = 11.43 (s, 2 H), 9.30 (d, J = 4.5 Hz 4 H), 9.27 (d, J = 5.0 Hz, 4 H), 9.24 (d, J = 4.5 Hz, 4 H), 9.20 (d, J = 5.0 Hz, 4 H), 9.03 (s, 2 H), 8.84 (s, 1 H), 8.58 (d, J = 7.8 Hz, 2 H), 8.35 (m, 12 H), 8.22 (d, J = 7.8 Hz, 2 H), 8.04 (s, 2 H), 7.78 (t, J = 7.8 Hz, 2 H), 7.60 (m, 12 H), 3.56 (s, 3 H), 2.92 (t, J = 7.7 Hz, 4 H), 2.88 (t, J = 7.7 Hz, 8 H), 1.82 (m, 12 H), 1.43 (m, 24 H), 0.97 (t, J = 6.6 Hz 6 H), 0.94 ppm (t, J = 6.6 Hz, 12 H); IR (KBr): $\tilde{\nu}$ = 3415, 2926,1617, 1526, 1384, 1339, 1207, 1000, 797, 720 cm^{-1}; HRMS (ESI): m/z calcd for $C_{127}H_{122}N_{10}O_3Zn_2Na$: 1989.8187; found: 1989.8273.

Zn–bisporphyrin 5c: Yield 94 %; m.p. 295–300 °C; ^{1}H NMR (300 MHz, $CDCl_3$): δ = 8.99 (s, 8 H), 8.98 (d, J = 5.3 Hz, 4 H), 8.96 (d, J = 5.3 Hz, 4 H), 8.26 (d, J = 8.5 Hz, 4 H), 8.19 (s, 2 H), 8.12 (d, J = 8.2 Hz, 4 H), 8.11 (d, J = 8.2 Hz, 8 H), 7.94 (d, J = 8.5 Hz, 4 H), 7.82 (s, 1 H), 7.57 (s, 2 H), 7.56 (d, J = 8.2 Hz, 4 H), 7.53 (d, J = 8.2 Hz, 8 H), 3.96 (s, 3 H), 2.95 (m, 12 H), 1.92 (m, 12 H), 1.50 (m, 24 H), 1.02 ppm (m, 18 H); IR (KBr): $\tilde{\nu}$ = 3409, 2924,1643, 1515, 1446, 1384, 1336, 1205, 1066, 796, 719 cm^{-1}; HRMS (ESI): m/z calcd for $C_{127}H_{122}N_{10}O_3Zn_2Na$: 1989.8187; found: 1989.8251.

Titrations and data analysis: ^{1}H NMR and UV-visible titrations were performed by adding solutions containing the ligand to a solution of the zinc porphyrin in either a 5 mm NMR tube or a 1 cm path cuvette by using microliter syringes. In both types of titration experiments the zinc–porphyrin was present in the guest solution at the same concentration as that in the NMR tube or cuvette to avoid dilution effects. Deacidified chloroform and deacidified deuterochloroform were used as solvents for the UV-visible and ^{1}H NMR titrations, respectively. In general, UV-visible spectrophotometric titrations were analyzed by fitting the whole series of spectra at 1 nm intervals by using the software SPECFIT 3.0 from Spectrum Software Associates (PMB 361, 197 M Boston Post Road West, Marlborough, MA 01752, USA), which uses a global system with expanded factor analysis and Marquardt least-squares minimization to obtain globally optimized parameters. Titration curves with respect to the simple binding model were also analyzed by fitting the data to the theoretically expected binding curve by using nonlinear curve-fitting programs developed by one of us (C.A.H.). In these simple cases the two methods gave similar results, but the first method was more accurate. In all the cases of the zinc–bis-porphyrins binding to DABCO, multivariate global factor analysis was the only method used. The reported errors for the stability constants directly calculated with SPECFIT, or any other fitting program, were estimated as the square root of the sum of the square of the standard deviations from at least three experimental values of the binding constants determined in different titration experiments. Errors for the stability constants and molarity effects computed using the values determined directly for the stability constants were estimated by error propagation analysis.[28]

Computational methods: Semiempirical calculations were carried out at the restricted Hartree–Fock (RHF) level using the AM1[29] method, as implemented in MOPAC-93 package.[30] The geometry of all structures was optimized and further refined by minimization of the gradient norm to less than 0.418 kJ Å^{-1} deg^{-1} by means of the Eigenvector Following (EF) routine.[31] Side chains were assumed not to be attached to the porphyrins in order to keep the size of the calculation approachable.

Acknowledgements

We thank the Dirección General de Investigación, Ministerio de Ciencia y Tecnología (MCyT) for grant support (BQU2002–04651). A.F. thanks MCyT for a "Ramón y Cajal" contract and A.M.C thanks the Ministerio de Educación for a predoctoral fellowship.

[1] a) P. N. Taylor, H. L. Anderson, *J. Am. Chem. Soc.* **1999**, *121*, 11538; b) J. S. Lindsey, *New J. Chem.* **1991**, *15*, 153; c) L. F. Lindoy, I. M. Atkinson, *Self-Assembly in Supramolecular Systems*, The Royal Society of Chemistry, Cambridge, UK, **2000**.

[2] B. J. Holliday, C. A. Mirkin, *Angew. Chem.* **2001**, *113*, 2076; *Angew. Chem. Int. Ed.* **2001**, *40*, 2022;

[3] S. Leininger, B. Olenyuk, P. J. Stang, *Chem. Rev.* **2000**, *100*, 853.

[4] a) C. M. Drain, J. D. Batteas, G. W. Flynn, T. Milic, N. Chi, D. G. Yablon, H. Sommers, *Proc. Natl. Acad. Sci. USA* **2002**, *99*, 6498; b) E. Iengo, E. Zangrando, E. Alessio, *Eur. J. Inorg. Chem.* **2003**, 2371; c) J. Wojaczynski, L. Latos-Grazynski, *Coord. Chem. Rev.* **2000**, *204*, 113; d) E. Alessio, E. Iengo, L. G. Marzilli, *Supramol. Chem.* **2002**, *14*, 103; e) Y. Kobuke, K. Ogawa, *Bull. Chem. Soc. Jpn.* **2003**, *76*, 689; f) L. Baldini, C. A. Hunter, *Adv. Inorg. Chem.* **2002**, *53*, 213.

[5] Examples of assemblies involving a metalloporphyrin unit acting simultaneously as donor and acceptor module: a) See reference [4e]; b) H.-J. Kim, N. Bampos, J. K. M. Sanders, *J. Am. Chem. Soc.* **1999**, *121*, 8120; c) A. Tsuda, H. Hu, R. Watanabe, T. Aida, *J. Porphyrins Phthalocyanines* **2003**, *7*, 388; d) A. Tsuda, S. Sakamoto, K. Yamaguchi, T. Aida, *J. Am. Chem. Soc.* **2003**, *125*, 15722.

[6] a) R. Takahashi, Y. Kobuke, *J. Am. Chem. Soc.* **2003**, *125*, 2372; b) C. Ikeda, N. Nagahara, N. Yoshioka, H. Inoue, *New J. Chem.* **2000**, *24*, 897; c) R. A. Haycock, C. A. Hunter, D. A. James, U. Michelsen, L. R. Sutton, *Org. Lett.* **2000**, *2*, 2435.

[7] a) K. Ogawa, Y. Kobuke, *Angew. Chem.* **2000**, *112*, 4236; *Angew. Chem. Int. Ed.* **2000**, *39*, 4070; b) U. Michelsen, C. A. Hunter, *Angew. Chem.* **2000**, *112*, 780; Angew . *Chem. Int. Ed.* **2000**, *39*, 764; c) C. Ikeda, E. Fujiwara, A. Satake, Y. Kobuke, *Chem. Commun.* **2003**, 616.

[8] a) X. Chi, A. J. Guerin, R. A. Haycock, C. A. Hunter, L. D. Sarson, *J. Chem. Soc. Chem. Commun.* **1995**, 2567; b) X. Chi, A. J. Guerin, R. A. Haycock, C. A. Hunter, L. D. Sarson, *J. Chem. Soc. Chem. Commun.* **1995**, 2563; c) G. Ercolani, *J. Phys. Chem. B* **2003**, *107*, 5052.

[9] a) C. C. Mak, N. Bampos, J. K. M. Sanders, *Angew. Chem.* **1998**, *110*, 3169; *Angew. Chem. Int. Ed.* **1998**, *37*, 3020; b) S. Yagi, M. Ezoe, I. Yonekura, T. Takagishi, H. Nakazumi, *J. Am. Chem. Soc.* **2003**, *125*, 4068; c) see also references [1a] and [11].

[10] a) C. A. Hunter, R. Tregonning, *Tetrahedron* **2002**, *58*, 691; b) L. Baldini, P. Ballester, A. Casnati, R. M. Gomila, C. A. Hunter, F. Sansone, R. Ungaro, *J. Am. Chem. Soc.* **2003**, *125*, 14181.

[11] a) H. L. Anderson, C. A. Hunter, M. N. Meah, J. K. M. Sanders, *J. Am. Chem. Soc.* **1990**, *112*, 5780; b) C. A. Hunter, M. N. Meah, J. K. M. Sanders, *J. Am. Chem. Soc.* **1990**, *112*, 5773; c) H. L. Anderson, *Inorg. Chem.* **1994**, *33*, 972; d) see also reference [1a].

[12] M. Gardner, A. J. Guerin, C. A. Hunter, U. Michelsen, C. Rotger, *New J. Chem.* **1999**, *23*, 309.

[13] S. B. Lee, J.-I. Hong, *Tetrahedron Lett.* **1998**, *39*, 4317.

[14] Stoichiometric binding constants for multiple site ligands are related to microscopic binding constants by means of statistical factors. See Figure 2 and reference [20], p. 20.

[15] It is generally accepted that intermolecular binding of a divalent receptor (two binding sites) to a monovalent substrate (unique binding site) is positively cooperative if α is larger than 1, it is non-cooperative or statistical if α is equal to 1, and it is negatively cooperative if α is smaller than 1. See reference [20], Chapter 2. α is calculated by dividing the value of the statistically corrected binding constant of the second interaction by that of the first interaction.

[16] SPECFIT, Version 3.0 from Spectra Software Associates: a) H. Gampp, M. Maeder, C. J. Meyer, A. D. Zuberbühler, *Talanta* **1986**, *33*, 943; b) H. Gampp, M. Maeder, C. J. Meyer, A. D. Zuberbühler, *Talanta* **1985**, *32*, 95.

[17] In order to use the same value of K_m for the three bisporphyrins we consider the cooperativity factor (α_P) in K_{11}. In this case, α is calculated by dividing the value of the statistically corrected binding constant of the first interaction by that of the second interaction. The system is said to be positively cooperative if α is smaller than 1.

[18] A. Osuka, K. Maruyama, *J. Am. Chem. Soc.* **1988**, *110*, 4454.

[19] C. A. Hunter, J. K. M. Sanders, A. J. Stone, *Chem. Phys.* **1989**, *133*, 395.

[20] K. A. Connors, *Binding Constants*, Wiley, New York, **1987**.

[21] a) A. J. Kirby, *Adv. Phys. Org. Chem.* **1980**, *17*, 183; b) L. Mandolini, *Adv. Phys. Org. Chem.* **1986**, *22*, 1.

[22] H. L. Anderson, S. Anderson, J. K. M. Sanders, *J. Chem. Soc. Perkin Trans. 1* **1995**, 2231.

[23] W. P. Jenks, *Catalysis in Chemistry and Enzymology*, Dover, New York, **1987**.

[24] Simulations of the species distribution during a titration with DABCO at millimolar concentration of the porphyrin using the association constants values calculated from the UV-visible titration and assuming a value of $K_{21}=4$ $K_m^2=3.2\times10^{10}\,M^{-1}$ for the stability constant of the ternary complex predict that at 0.5 equivalents of DABCO, the ratio of ternary/sandwich complex should be 15/85, 1/99, and 11/89 for **5a**, **5b**, and **5c**, respectively.

[25] The distribution profiles of Figure 11 were simulated as in Figure 9, but at a higher concentration of **5a–c**. The good fit of the experimental data obtained at millimolar concentration with the distribution profile, simulated using stability constants measured at micromolar concentrations, suggests that there is no change of the binding mode over this concentration range. This simplification implies the exclusive formation of a sandwich complex of unique stoichiometry (1:1 or 2:2) for each binding model. The binding constants obtained for the fitting of the UV-visible titration data of **5c** to the exclusive formation of a 3:3 sandwich complex are log $K_{33}=32.5$; log $K_{21}=10.5$. These values were used in the simulation of the distribution profile for the destruction of a 3:3 sandwich complex as presented in Figure 11c.

[26] Experiments to distinguish the structure of the complexes by ESI mass spectrometry gave only molecular ions corresponding to the free porphyrins. This is a common result for supramolecular assemblies based on the coordination of zinc–oligoporphyrins with aza ligands. All attempts to grow crystals were unsuccessful.

[27] H. Zhao, A. Thurkauf, *Synth. Commun.* **2001**, *31*, 1921.

[28] J. R. Taylor, *An Introduction to Error Analysis: The Study of Uncertainity in Physical Measurements*, University Science Books, Mill Valley, CA, **1982**.

[29] M. J. S. Dewar, M. E. G. Zoebisch, E. F. Healy, J. J. P. Stewart, *J. Am. Chem. Soc.* **1985**, *107*, 3902.

[30] J. J. P. Stewart, MOPAC-93, Fujitsu, **1993**

[31] J. Baker, *J. Comput. Chem.* **1986**, *7*, 385.

Received: July 28, 2004
Revised: November 19, 2004
Published online: February 16, 2005